Ambient noise surface wave tomography of South China

Longquan Zhou[1], Yong Zheng[2], Weisen Shen[3], Yingjie Yang[4], Haixia Shi[1], and Michael H. Ritzwoller[3]

1. China Earthquake Network Center, Beijing, 100045, China (lqzhou@seis.ac.cn)

2. Key Laboratory of Dynamic Geodesy, Institute of Geodesy and Geophysics, Chinese Academy of Sciences, Wuhan, Hubei, 430077, China (zhengyong@whigg.ac.cn)

3. Center for Imaging the Earth's Interior, Department of Physics, University of Colorado at Boulder, Boulder, CO 80309-0390 USA (michael.ritzwoller@colorado.edu)

4. Department of Earth and Planetary Sciences, Macquarie University, 2109 Sydney Australia (yingjie.yang@mq.edu.au)

[1] Two years of continuous recordings of ambient seismic noise observed at 425 stations in South China in the years 2009 and 2010 are used to estimate Rayleigh wave group and phase velocity maps from 6 to 50 sec period. These maps place new constraints on crustal thickness and shear wave speeds from the shallow crust into the uppermost mantle. The paleo-architecture of the South China Block is reflected in the maps at short periods where the Yangtze Craton and South China Foldbelt are distinguishable. At longer periods, however, the dispersion maps are dominated by east-west variations, which largely reflect the influence of recent tectonics including crustal thickening and reduction of crustal shear wave speeds in the western Yangtze Craton and Youjian Block. In addition, the South China Foldbelt has a much thinner crust and a thinner lithosphere than the Yangtze Craton, on average.

1. Introduction

[2] The recent tectonic evolution of eastern Asia has been driven by subduction to the

east and continental collision to the west. Eastern China is a fairly passive participant in this neo-tectonic framework, having formed no later than the early Paleozoic. The paleo-architecture of Eastern China is dominated by two crustal blocks, the Sino-Korean (or North China) Craton and the South China Block, which are separated by the Qinling-Dabie-Sulu orogenic belt. The South China Block was formed by the collision between the Yangtze Craton and the Cathasyia Block [*e.g., Zheng et al., 2006*], which itself is composed of the South China Foldbelt and the younger Youjiang Block [*Zhang et al., 2003*]. (See Figure 1a.) The Sino-Korean and Yangtze Cratons are both Archean in age, but the geological structure of the Yangtze Craton is more poorly understood because it is largely shrouded in Precambrian strata [*Lebedev & Nolet*, 2003]. The Yangtze Craton encompasses two large sedimentary basins, the Jianghan Basin and the Sichuan Basin, which may have formed the nucleus of formation for the Yangtze Craton [*Zhang et al., 1984*]. The South China Block is tectonically stable and suffers few earthquakes, except along its northern margin and western margin where it presents an obstacle to eastern mass transport from the Tibetan Plateau [*e.g., Royden et al.,*1997] and numerous large earthquakes occur [*e.g., Zhang et al.,* 2003].

[3] A number of factors have inhibited the seismic imaging of the crust and upper mantle beneath the South China Block, including the lack of seismicity and poor station coverage historically. At least parts of the South China Block have been imaged by larger scale tomographic studies, including *Ritzwoller and Levshin* [1998], *Ritzwoller et al.* [1998], *Lebedev and Nolet* [2003], *Huang et al*. [2003], and *Zheng et*

al. [2008]. By the end of 2007, however, a new digital seismic observing system was completed in China [*Zheng et al.*, 2010a], which has been used in P-wave travel time tomography [e.g., *Li and van der Hilst,* 2010] and surface wave tomography in neighboring regions [*e.g., Yang et al., 2010; Zheng et al.,* 2010b, 2011]. This observing system in South China consists of 425 seismic stations equipped with very broadband (VBB), ultra broadband (UBB), or broadband (BB) seismometers (Figure 1b). We present here a new step in imaging the crust and uppermost mantle beneath the South China Block: Rayleigh wave ambient noise tomography in South China extending from periods of 6 to 50 sec. The resolution of structures in South China that emerges is unprecedented.

2. Data and Methods

[4] The use of ambient noise to extract surface wave empirical Green's functions (EGFs) and to infer Rayleigh wave [e.g., *Sabra et al.,* 2005; *Shapiro et al.*, 2005] group and phase speeds in continental areas is well established [e.g., *Bensen et al.,* 2007; *Lin et al.,* 2008]. The resolution of ambient noise tomography is limited only by the number, distribution, and quality of stations. We process two years of continuous vertical component ambient noise observed at 425 seismic stations in South China, so the cross-correlations predominantly contain only Rayleigh waves.

[5] The data processing procedures we adopt here follow those of *Bensen et al.* [2007] and *Lin et al.* [2008]. Continuous data are decimated to one sample per sec and then filtered in the period band from 5 to 50 sec. Instrument responses are then removed from the continuous data because different types of seismic sensors are used; most are

BB (long period corner at 20 sec) but some are VBB (120 sec corner) or UBB (360 sec corner). Time-domain normalization in a running window 80 seconds in length is applied to suppress the influence of earthquake signals and other irregularities and spectral whitening is applied to flatten spectra over the entire period band (5-50 sec). After completing these processing steps, cross-correlations are performed daily between pairs of stations in the period band from 5-50 sec and then are stacked over the two-year time window.

[6] Figure 2 displays an example cross-correlation record section between Chinese station AHJIX and other stations in South China. Strong surface wave signals are observed on both positive and negative correlation lags. To simplify data analysis and enhance the signal-to-noise ratio (SNR) of the surface waves, we separate each cross correlation into positive and negative lag components and then add the two components to form the so-called"symmetric component."

[7] Group and phase velocity dispersion measurements of Rayleigh waves are obtained from the symmetric components of inter-station cross-correlations by automatic frequency-time analysis (FTAN) [*Bensen et al.*, 2007]. Group velocity is measured on the envelope of the surface wave packet and phase velocity measurements are made on the phase content of the wave packet. Group and phase velocity are not constrained to agree although they are related theoretically [e.g., *Levshin et al.*, 1999]. The automated FTAN dispersion measurements are winnowed by applying three criteria to select reliable measurements for surface wave tomography. (1) The distance between two stations must be greater than three

wavelengths for group velocity and two wavelengths for phase velocity to ensure sufficient separation of the surface wave packets from precursory noise. (2) SNR must be greater than 15 at each period for the measurement at that period to be accepted. (3) We require that the measurements agree with one another across the data set. Measurements that can be fit well by a smoothed tomographic map are considered to cohere within the data set as a whole, otherwise they are rejected.

[8] In principle, 425 stations could produce up to about 90,000 cross-correlations. The smaller numbers presented in Table 1 reflects the strength of ambient noise (which reduces above ~20 sec period) and the pass-band of the China Provincial stations (which falls off above ~20 sec period for BB data). Also, at periods below ~10 sec, scattering from small-scale heterogeneities make measurement of surface wave speeds more difficult. In step (3) of data selection, travel time errors of π and 2π are identified and either corrected or removed from the data set. Group velocity measurements generally outnumber phase velocity measurements because of data rejection caused by π and 2π errors that affect the phase but not the group velocity measurements.

[9] We perform surface wave tomography on the selected dispersion measurements to produce Rayleigh wave group and phase velocity maps on a 0.5° by 0.5° grid using the straight ray tomography method of *Barmin et al*. [2001]. The relatively short paths that are considered here will not be strongly affected by off-great circle effects except at short periods near the Sichuan Basin [e.g., *Lin et al.,* 2009] and finite frequency effects will also be weak in the period band of study [*Lin and Ritzwoller,* 2011].

Resolution is simultaneously estimated at each period.

[10] Misfit statistics based for the final tomographic maps provide information about the quality of the dispersion measurements. Below 20 sec period, in the primary pass-band of Chinese BB instruments, phase travel time misfit is about 1 second and group travel time misfit is several times larger, the typical relationship between phase and group travel time misfits. Misfit degrades below 10 sec due to scattering from small-scale heterogeneities and above 20 sec because of reduction in signal level as the instrument response rolls off and because paths are typically longer, on average. Overall, misfit statistics establish that data quality is very high, particularly between 10 and 20 sec period where it is similar to misfits derived from USArray data in the US [e.g., *Lin et al.*, 2008].

3. Dispersion Maps

[11] Rayleigh wave group and phase velocity maps are produced on a 2 sec period grid from 6 sec to 20 sec period and then on a 5 sec period grid to 50 sec period. Examples of these maps at 8, 14, 20 and 30 sec period are shown in Figures 3 and 4. Velocity perturbations are plotted only where resolution is better than 200 km. Resolution is defined as twice the standard deviation of a 2-D Gaussian fit to the resolution surface at each geographic node [*Barmin et al.* 2001]. At each period, the group velocity anomalies are sensitive to shallower structures than the phase velocities. Thus, for example, phase velocity maps should be compared with longer period group velocity maps.

[12] The short period maps, e.g., 8 and 14 sec group velocity and 8 sec phase velocity,

are strongly influenced by the shallow part of the crust, particularly the existence of sediments. The major sedimentary basins, such as the Sichuan Basin, Jianghan basin, North China Plain, North Jiangsu Basin, and the South China Sea between the mainland and Hainan Island, all appear as low velocities. The boundary between the South China Block and the North China Carton is clear because of sediments deposited near boundary of these regions. The 14 sec group velocity map also shows a clear distinction between the South China Foldbelt and the generally faster Yangtze Craton. At short periods, the Youjian Block is not distinguishable from the South China Fold Belt.

[13] At longer periods, 20 sec and above, the maps are affected by mid- to lower-crustal shear wave speed and at the longest periods by crustal thickness. At these periods, the velocity features lose the tectonic coherence seen at shorter periods; the predominant structure is a west to east velocity variation. On the 30 sec group velocity and the 20 sec phase velocity maps, for example, the Yangtze Craton is roughly bifurcated, being slow in the west and fast in the east. This is probably due to the influence of Tibet and the resulting thicker crust in the west [*Zhang et al.*, 1984; *Teng et al.*, 2003]. At these periods, the Youjian Block becomes distinguishable from the South China Foldbelt, probably again because of the influence of active tectonics in the west. However, the eastern Yangtze Craton and South China Foldbelt are not distinguishable, consistent with the expectations or results of earlier studies [*Li and Mooney*, 1998; *Huang et al*. 2003].

[14] The deepest sensitivity of these maps is provided by the 30 sec phase velocity

map, which is qualitatively similar to longer period maps up to 50 sec. These maps are strongly sensitive to crustal thickness where thicker crust appears as lower velocities. The sedimentary basins appear predominantly as high velocity features on this map, which is common for sedimentary basins around the world. In addition, the South China Foldbelt is generally faster than the eastern Yangtze Craton, reflective of thinner crust as discussed in section 4. Finally, very low velocities are imaged for the Bayan Har, Chuandian, and South Yunnan Blocks, which are expected for these actively deforming regions with thicker crust (section 4).

4. Discussion

[15] The paleo-architecture of the South China Block varies predominantly in the north-south direction. These variations are primary observed at short periods where the Yangtze Craton and South China Foldbelt are distinguishable (e.g., Fig 3b). At longer periods, the dispersion maps are dominated by east-west variations, which largely reflect recent tectonic influences. These trends are seen more clearly in the local dispersion curves and shear velocity (V_s) model constructed by Monte-Carlo inversion [e.g., *Shapiro and Ritzwoller,* 2002]. Presenting the full 3-D V_s model is beyond the scope of this paper, but example profiles to 80 km depth beneath the Chuandian Block, the Sichuan Basin, the Yangtze Craton, and the South China Foldbelt are shown in Figure 5. Selected features of these four profiles are summarized in Table 2.

[16] The crust is thicker in the western part of the study region being roughly the

same inside (~43±6 km) and outside (~42±5 km) the Sichuan Basin within the western Yangtze Craton. The crust of the Chuandian Block is much thicker (~52±6 km) and that of the South China Foldbelt much thinner (~31±4 km) than the Yangtze Craton. Sediments in the Sichuan Basin are estimated to have a thickness of 5±2 km. The Yangtze Craton and South China Foldbelt have similar shear wave speeds in the lower crust (3.60-3.65 km/s), but the lower crust of the Sichuan Basin is much faster (3.74±0.04 km/s) and that of the Chuandian Block much slower (3.42±0.04 km/s). Uppermost mantle wave speeds at 80 km depth beneath the Sichuan Basin and western Yangtze Craton are similar (~4.7±0.1 km/s), but are much slower beneath the Chuandian Block (4.44±0.12 km/s) and South China Foldbelt (4.34±0.1 km/s) indicating a thinner lithosphere beneath these structures. Thus, compared with the Yangtze Craton the South China Foldbelt has a much thinner crust and a thinner lithosphere whereas the Chuandian Block has a thicker crust but thinner lithosphere.

[17] The presentation of a full 3-D model for South China will await extension of the analysis to longer periods by introducing earthquake data via multi-plane wave [*Yang et al.*, 2008], eikonal [*Lin et al.*, 2009], or Helmholtz [*Lin and Ritzwoller,* 2011] tomography in order to improve constraints on crustal thickness and uppermost mantle structure.

Acknowlegments

All waveform data used were obtained from the Data Management Centre of the China National Seismic Network at the Institute of Geophysics, China Earthquake

Administration. This work was supported by US NSF-EAR award 0944022, US NSF-OISE sub-award 0730154, the National Natural Science Foundation of China (41004036, 40974034).

References

Barmin, M. P., M. H. Ritzwoller, and A. L. Levshin (2001), A fast and reliable method for surface wave tomography, *Pure Appl. Geophs*., 158:1351-1375.

Bensen, G. D., M. H. Ritzwoller, M. P. Barmin, A. L. Levshin, F. Lin, M. P. Moschetti, N. M. Shapiro, and Y. Yang (2007), Processing seismic ambient noise data to obtain reliable broad-band surface wave dispersion measurements, *Geophys. J. Int.*, 169: 1239-1260.

Huang, Z. X., W. Su, Y. J. Peng, Y. J. Zheng, and H. Y. Li (2003), Rayleigh wave tomography of China and adjacent regions, *J. Geophys. Res.*, 108, doi:10.1029/2001JB001696.

Lebedev, S., and G. Nolet (2003), Upper mantle beneath Southeast Asia from S velocity tomography, *J. Geophys. Res.*, 108, doi:10.1029/2000JB000073.

Levshin, A.L., M.H. Ritzwoller, and J.S. Resovsky (1999), Source effects on surface wave group travel times and group velocity maps, *Phys. Earth Planet. Int.*, 115, 293 - 312.

Li, C. and R.D. van der Hilst (2010), Structure of the upper mantle and transition zone beneath Southeast Asia from traveltime tomography, J. Geophys. Res., 115, B07308, doi:1029/2009JB006882.

Li, S.L. and W. D. Mooney (1998), Crustal structure of China from deep seismic sounding profiles, *Tectonophysics*, 288, 105-113.

Lin, F.C., M.P. Moschetti, and M.H. Ritzwoller (2008), Surface wave tomography of the western United States from ambient seismic noise: Rayleigh and Love wave phase velocity maps, *Geophys. J. Int.*, doi:10.1111/j1365-246X.2008.03720.x.

Lin, F.C., M.H. Ritzwoller, and R. Snieder (2009), Eikonal Tomography: Surface wave tomography by phase-front tracking across a regional broad-band seismic array, *Geophys. J. Int.*, 177(3), 1091-1110.

Lin, F.C. and M.H. Ritzwoller (2011), Helmholtz surface wave tomography for isotropic and azimuthally anisotropic structure, *Geophys. J. Int.*, in press.

Ritzwoller, M.H. and A.L. Levshin (1998), Eurasian surface wave tomography: Group velocities, *J. Geophys. Res.*, 103, 4839 - 4878.

Ritzwoller, M.H., A.L. Levshin, L.I. Ratnikova, and A.A. Egorkin (1998), Intermediate period group velocity maps across Central Asia, Western China, and parts of the Middle East, *Geophys. J. Int.*, 134, 315-328.

Royden, L. H., B.C. Burchfiel, et al. (1997), Surface deformation and lower crustal flow in eastern Tibet. *Science*, 276:788-790.

Sabra, K. G., P. Gerstoft, P. Roux, W. A. Kuperman, and M. C. Fehler (2005), Surface wave tomography from microseisms in Southern California, *Geophys. Res. Lett.* 32, L14311.

Shapiro, N.M. and M.H. Ritzwoller (2002), Monte-Carlo inversion for a global shear velocity model of the crust and upper mantle, *Geophys. J. Int.*, 151, 88-105.

Shapiro, N. M., M. Campillo, L. Stehly, and M. H. Ritzwoller (2005), High-resolution surface wave tomography from ambient seismic noise. *Science* 307, 1615-1618.

Teng, J. W., R. S. Zeng, Y. F. Yan, and H. Zhang (2003), Depth distribution of Moho and tectonic framework in eastern Asian continent and its adjacent ocean areas, *Science in China, Ser. D*, 46(5), 428-446.

Yang, Y., M.H. Ritzwoller, F.-C. Lin, M.P. Moschetti, and N.M. Shapiro (2008), The structure of the crust and uppermost mantle beneath the western US revealed by ambient noise and earthquake tomography, *J. Geophys. Res.*, 113, B12310.

Yang, Y., Y. Zheng, J. Chen, S. Shou, S. Celyan, E. Sandvol, F. Rilmann, K. Priestley, T.M. Hearn, J.F. Ni, L.D. Brown, and M.H. Ritzwoller (2010), Rayleigh wave phase velocity maps of Tibet and the surrounding regions from ambient seismic noise tomography, *Geochem., Geophys., Geosys.*, 11(8), Q08010, doi:10.1029/2010GC003119.

Zhang, P. Z., Q. D. Deng, G. M. Zhang, J. Ma, W. J. Gan, W. Min, F. Y. Mao, and Q. Wang (2003), Active tectonic blocks and strong earthquakes in the continent of China, *Science in China, Ser. D*, 46(Supp.), 13-24.

Zhang, Z. M., J. G. Liou, and R. G. Coleman (1984), An outline of the plate tectonics of China, *Geol. Soc. Am. Bull*, 95, 295-312.

Zheng, J., W.L. Griffin, S.Y. O'Reilly, M. Zhang, N. Pearson, and Y. Pan (2006), Widespread Archean basement beneath the Yangtze craton, *Geology*, 34(6), 417-420, doi:10.1130/G22282.1.

Zheng, S., X. Sun, X. Song, Y. Yang, and M.H. Ritzwoller, Surface wave tomography of China from ambient seismic noise, *Geochem. Geophys. Geosyst.*, 9, Q0502, doi:10.1029/2008GC001981, 2008.

Zheng, X. F., Z. X. Yao, J. H. Liang, and J. Zheng (2010a), The role played and opportunities provided by IGP DMC of China National Seismic Network in Wenchuan earthquake disaster relief and researches, *Bull. Seismol. Soc. Am.*, 100(5B), 2866-2872.

Zheng, Y., Y. Yang, M.H. Ritzwoller, X. Zheng, X. Xiong, Z. Li (2010b), Crustal structure of the northeastern Tibetan Plateau, the Ordos Block, and the Sichuan Basin from ambient noise tomography, *Earthquake Science*, 3, 465-476, doi:10.1007/s11589-010-0745-3.

Zheng, Y., W. Shen, Y. Yang, Z. Xie, M.H. Ritzwoller (2011), Ambient noise Rayleigh wave tomography for northeast China, the Korean Peninsula, and the Sea of Japan, in preparation.

Figure Captions:

Figure 1. (a) Tectonic map of South China. Thick lines indicate the boundaries of the major tectonic units and basins, after *Zhang et al*. [1984] and *Zhang et al* [2003]. The South China Block comprises the Yangtze Craton, which encompasses the Sichuan Basin (**SB**) and the Jianghan Basin (**JB**), the South China Foldbelt, and the Youjian Block (**YB**). Other identified tectonic features are: **OB**, Ordos Basin; **NCP**, North China plain; **NJB**, North Jiangsu Basin; **BHB**, Bayan Har Block; **CB**, Chuandian Block; **SYB**, South Yunnan Block; **YB**, Youjiang Block. The four diamonds identify locations referred to in Fig. 5. (b) The 425 broadband China Provincial Seismic Network stations (red triangles) used in this study. The blue triangle is the location of station AHJIX referred to in Fig. 2.

Figure 2. Two-year cross-correlations filtered between periods of 5 and 50 sec are shown between seismic station AHJIX (blue triangle in Fig. 1b) and other stations. Rayleigh waves appear at both negative and positive correlation lag times with a move-out of about 3 km/s. Arrivals near zero time are probably mostly teleseismic body waves, which are not studied here.

Figure 3. Rayleigh wave group velocity maps at periods of 8, 14, 20 and 30 sec. Maps truncate (revert to grey shades) where resolution is worse than 200 km. Average group velocities at these periods are 2.9488 km/s, 2.9177 km/s, 2.9514 km/s and 3.2937 km/s, respectively.

Figure 4. Rayleigh wave phase velocity maps at periods of 8, 14, 20 and 30 sec. As in Fig. 3, maps truncate where resolution is worse than 200 km. Average group velocities at these periods are 3.1335 km/s, 3.2854 km/s, 3.4748 km/s, 3.7141 km/s, respectively.

Figure 5. Dispersion curves and inferred V_s profiles at different locations: Chuandian Block, Sichuan Basin, Yangtze Craton, and South China Foldbelt. Locations are indicated by the green, black, blue, and red diamonds in Fig. 1a, respectively. (Top Row) Rayleigh wave phase (red lines) and group (blue lines) velocities predicted from the best fitting V_s model are compared with the measured values (error bars) extracted from the dispersion maps at each location. Square-root of χ^2 misfit is listed as "RMS misfit". (Middle Row) Shallow V_s structure: 2σ corridor of acceptable models between the surface and 25 km depth, highlighting the shallow crust. (Bottom Row) Full V_s model: 2σ corridor of acceptable models between the surface and 80 km depth, highlighting crustal thickness (dashed line).

Table 1. Final number of measurements and misfit.

Period (sec)	Number of measurements		Final Misfit (sec)	
	Group	Phase	Group	Phase
6.00	14245	14016	1.96	1.37
8.00	19776	19485	2.33	1.43
10.00	26008	24513	2.67	1.12
12.00	28761	27014	2.86	0.98
14.00	30255	28361	2.93	0.93
16.00	31082	29326	3.33	1.12
18.00	30350	28540	3.78	1.12
20.00	27561	25947	4.02	1.12
25.00	18940	17769	4.62	1.26
30.00	11913	11186	4.75	1.42
35.00	7257	6905	5.09	1.62
40.00	4849	4592	5.39	1.77
45.00	3135	3002	5.24	1.87
50.00	2086	1974	5.51	1.94

Table 2. Summary characteristics of models shown in Fig. 5. Uncertainties are 2σ for velocities and 1σ for sediment and crustal thickness.

	Chuandian Block	Sichuan Basin	Yangtze Craton	South China Foldbelt
Thickness, sediments	0.44 ± 0.30 km	5.26 ± 1.70 km	0.98 ± 0.53 km	0.21 ± 0.12 km
Thickness, crust	51.99 ± 5.7 km	43.00 ± 6.22 km	42.18 ± 4.86 km	31.12 ± 3.71 km
V_s, 20km	3.42 ± 0.04 km/s	3.74 ± 0.04 km/s	3.65 ± 0.04 km/s	3.60 ± 0.04 km/s
V_s, 80km	4.44 ± 0.12 km/s	4.70 ± 0.10 km/s	4.68 ± 0.09 km/s	4.34 ± 0.09 km/s

Figure 1

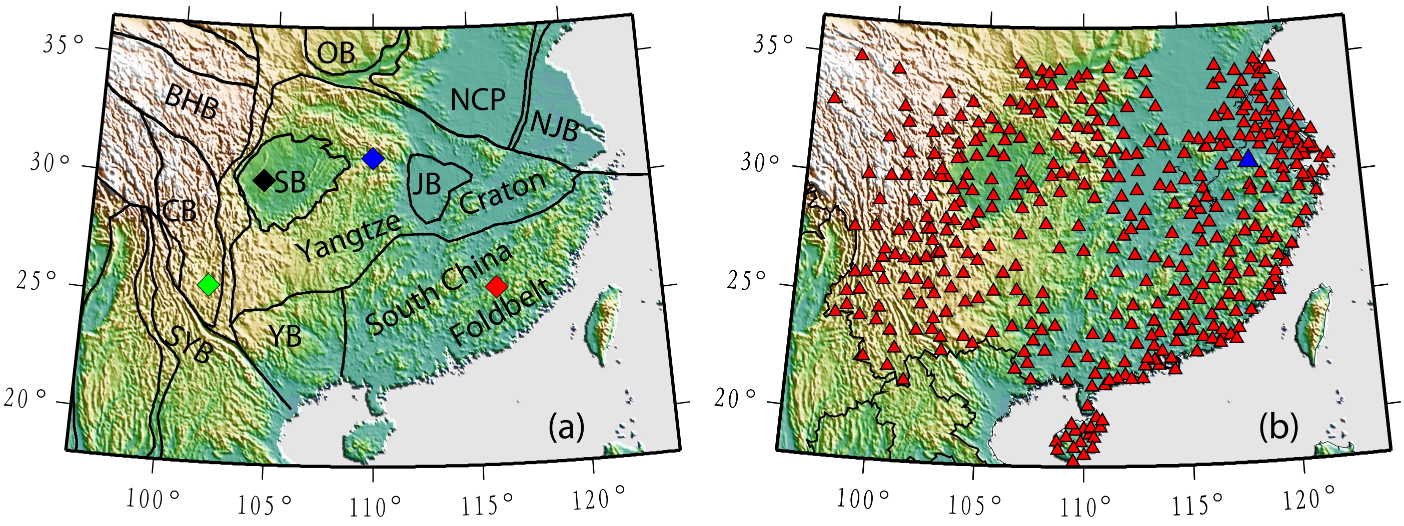

35°
30°
25°
20°
100°
105°
110°
115°
120°
OB
BHB
NCP
NJB
SB
JB
Craton
CB
Yangtze
South China
Foldbelt
SYB
YB
(a)
(b)

Figure 2

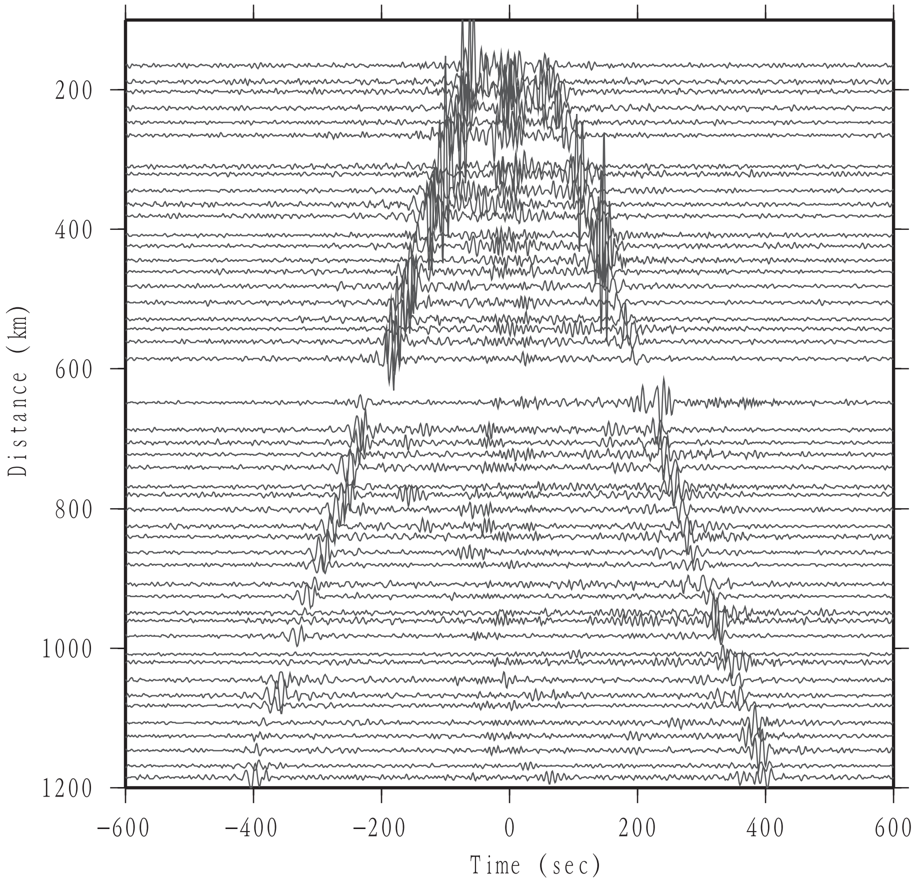

200
400
600
800
1000
1200
Distance (km)
-600
-400
-200
0
200
400
600
Time (sec)

Figure 3

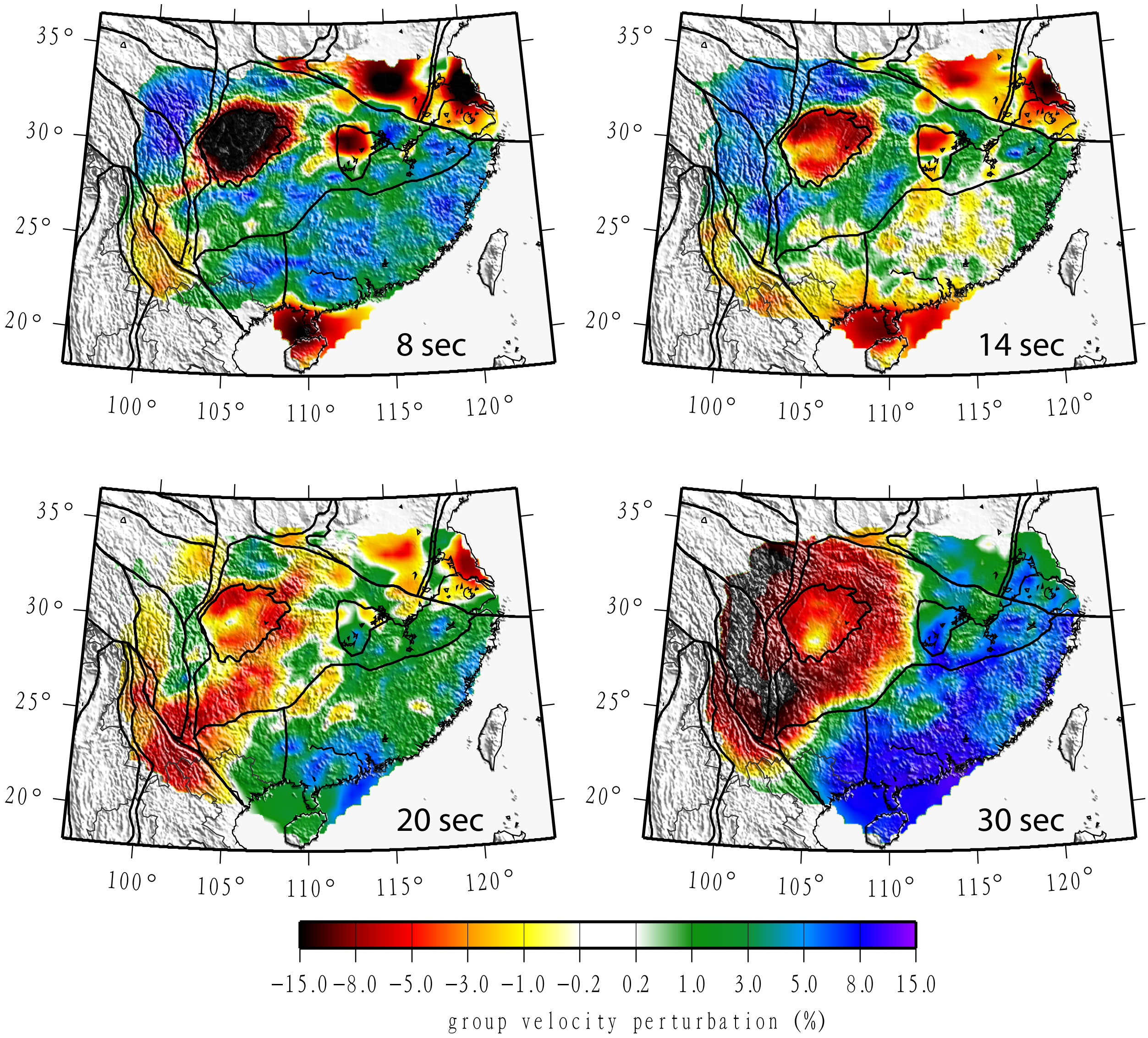
35°
30°
25°
20°
100°
105°
110°
115°
120°
8 sec
14 sec
20 sec
30 sec
−15.0 −8.0 −5.0 −3.0 −1.0 −0.2 0.2 1.0 3.0 5.0 8.0 15.0
group velocity perturbation (%)

Figure 4

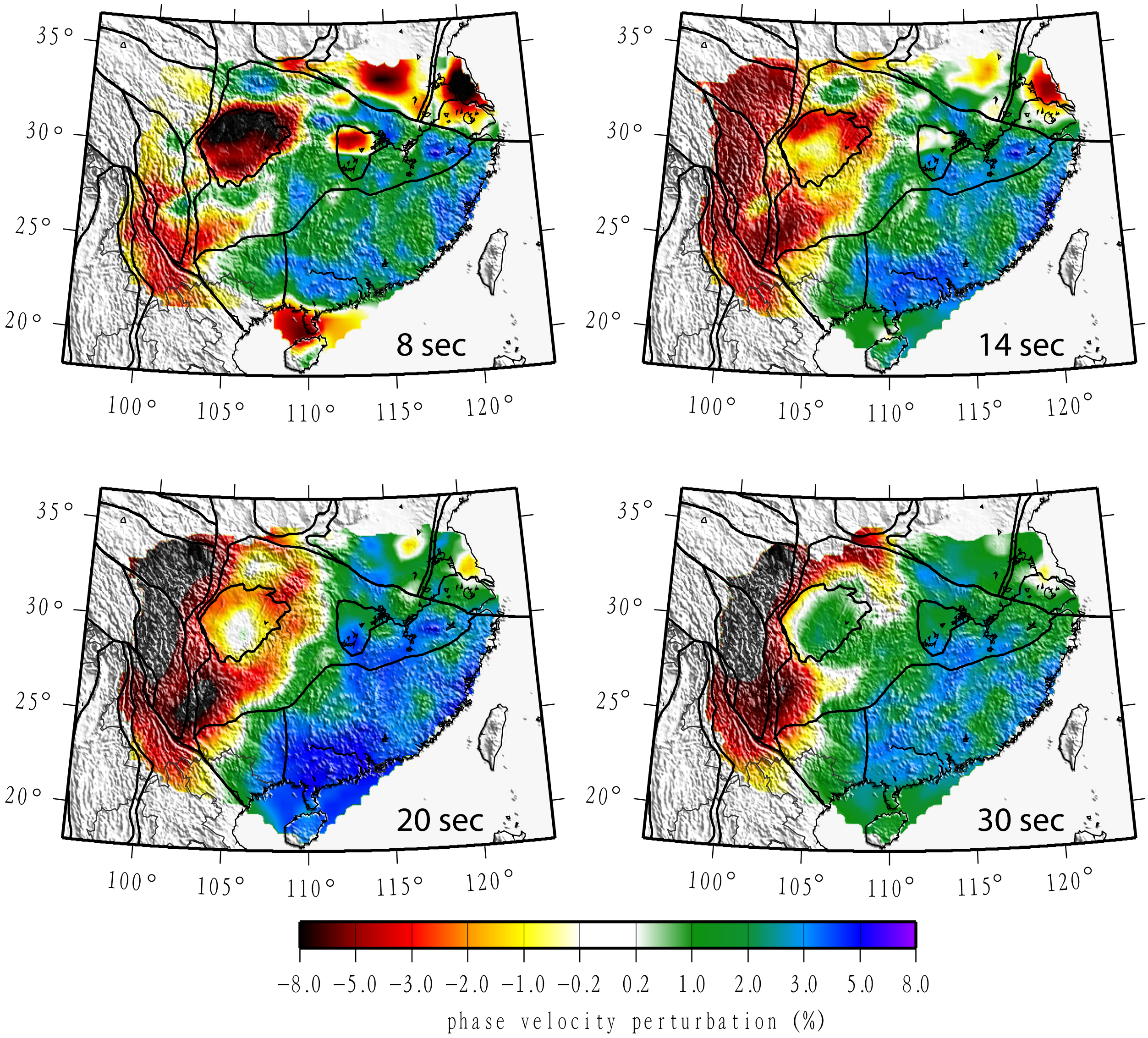

35°
30°
25°
20°
100°
105°
110°
115°
120°
8 sec
14 sec
20 sec
30 sec
-8.0 -5.0 -3.0 -2.0 -1.0 -0.2 0.2 1.0 2.0 3.0 5.0 8.0
phase velocity perturbation (%)

Figure 5

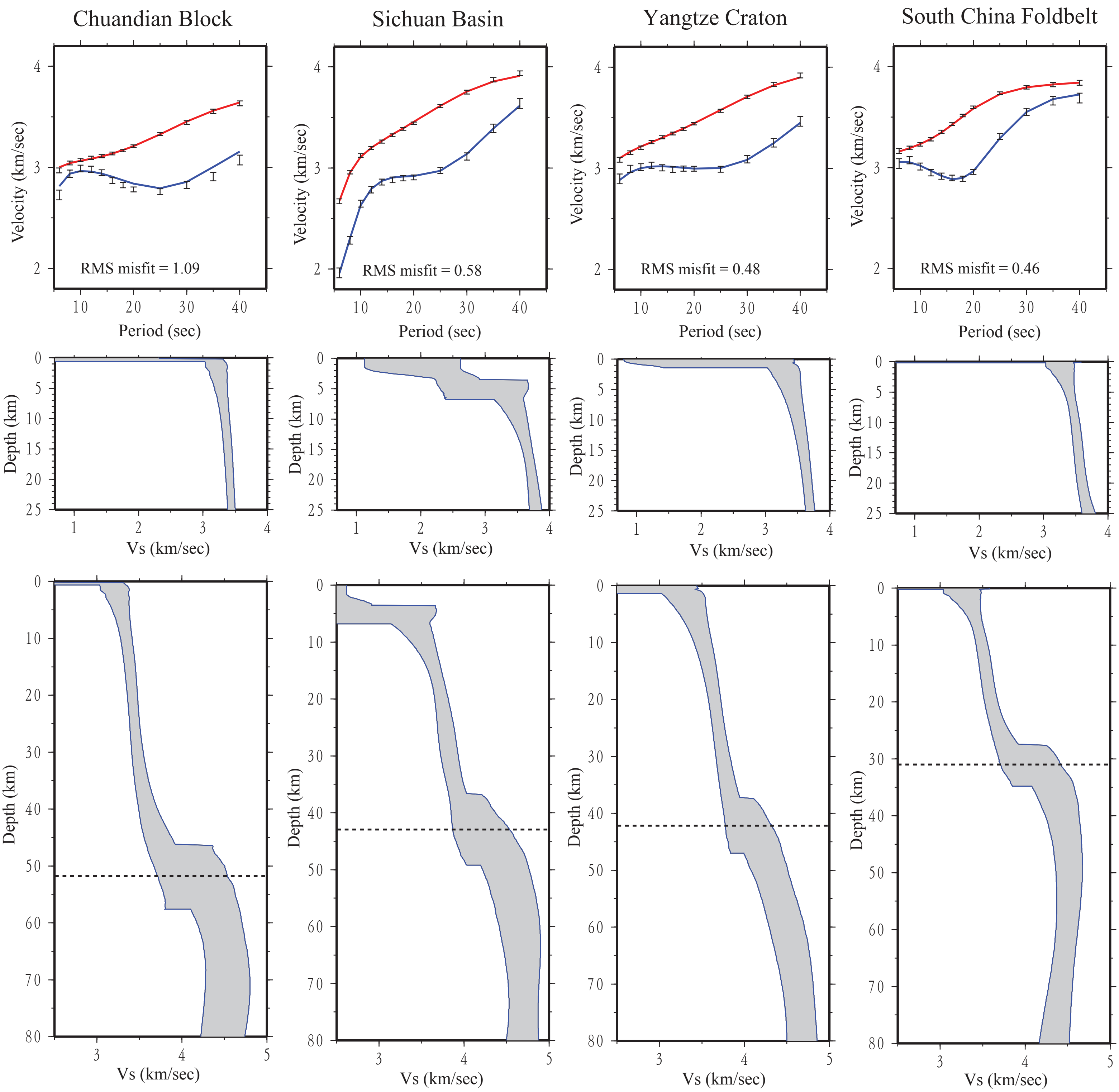

Chuandian Block
Sichuan Basin
Yangtze Craton
South China Foldbelt
Velocity (km/sec)
Period (sec)
RMS misfit = 1.09
RMS misfit = 0.58
RMS misfit = 0.48
RMS misfit = 0.46
Depth (km)
Vs (km/sec)